Force Balance at the Transition from Selective Withdrawal to Viscous Entrainment

François Blanchette* and Wendy W. Zhang
The Physics Department & James Franck Institute, University of Chicago, Chicago, Illinois 60637, USA
(Received 9 July 2008; published 7 April 2009)

We simulate the evolution of the steady-state interface in the selective withdrawal regime. Selective withdrawal ends when the upward pull exerted by the viscous flow in the withdrawing liquid layer overcomes the downward force due to surface tension. The lower-layer dynamics are unimportant. The dominant contribution to the surface-tension force comes from the large area where the interface is weakly deflected, instead of the small area where the surface is most distorted. A scaling estimate based on this idea yields results that agree quantitatively with both simulations and previous experiments.

DOI: 10.1103/PhysRevLett.102.144501 PACS numbers: 47.55.nm, 47.15.G−

While shape transitions driven by equilibrium dynamics are rather well understood, analogous transitions driven by nonequilibrium effects remain active areas of research [1–9]. Here we examine a simple example of shape transition driven by viscous flow. Viscous withdrawal in two immiscible, stratified liquid layers produces a shape transition from a hump to a spout. Figure 1(a) gives two images from the experiment of [4]. A tube is inserted into the upper layer and suspended above the interface. Liquid is withdrawn through the tube at a fixed volumetric rate and replenished far away from the surface. This withdrawal creates an axisymmetric flow in the upper layer which converges inwards radially and extends axially. The viscous stress exerted by the withdrawal flow pulls the interface upwards. When Q, the volume flux of liquid withdrawn through the tube, is small, the interface forms a hump directly under the tube. Above a threshold value Q_c, the hump is replaced by a spout that is drawn from the lower layer into the withdrawal tube. The selective withdrawal regime, in which only liquid from the upper layer is withdrawn, is thus succeeded by the viscous entrainment regime, in which liquid from both layers are withdrawn.

Both the stresses due to the fluid flow and those due to surface tension act on the fluid surface. Two feedback mechanisms are therefore present in the fluid problem. First, when the withdrawal flow in the upper layer deforms the surface, the change in the surface shape in turn modifies the withdrawal flow. Second, the flow in the upper layer induces a recirculating flow in the lower layer. The viscous stress generated by this lower-layer recirculation can also modify the withdrawal flow. Naively, one would expect both feedback mechanisms to be relevant in shaping the interface. However, measurements of Q_c for different pairs of liquids show little dependence on the viscosity of the lower-layer liquid [10]. Moreover, the measured dependencies of Q_c on S_p, the suspension height of the tube, appear to support two different scaling laws: an S_p^3 scaling consistent with an estimate obtained by Lister for viscous withdrawal of two liquids with equal viscosities [3], and a S_p^2 behavior. For a specific withdrawal experiment, it was not clear what factors control which scaling law is attained. From those experimental results, it was also unclear whether the shape transition is discontinuous, or continuous, corresponding to the tip of the hump sharpening until becoming singular at Q_c [4,10]. Kleine Berkenbusch, Cohen, & Zhang [11] used a combination of simulations and experiments to examine the transition for two liquids of equal viscosity. Their results demonstrate that, as Q increases towards Q_c, the steady-state solution for the hump disappears via a saddle-node bifurcation. The transition is discontinuous, with the hump shape remaining smooth at Q_c.

Motivated by these results, we reexamine the approach to transition. Consistent with the experiments, the numerical results for different pairs of liquids show clearly that the feedback mechanism involving the interaction of the upper and lower layer is unimportant. This simplification results from the fact that the stabilizing surface tension force is dominated by the contribution from the large area where

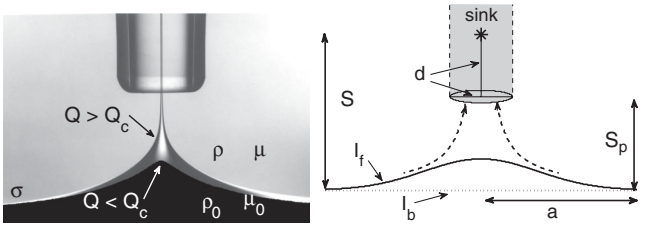

FIG. 1. (a) Selective withdrawal and viscous entrainment regimes (superposed images). Liquid is withdrawn at volume flux Q through a tube suspended above the interface separating two viscous, immiscible liquids. Below Q_c, the interface shape is a steady-state hump (black). Above Q_c, a spout forms (grey). The lower-layer liquid has viscosity μ_0 and density ρ_0; the upper layer has viscosity μ and density ρ. The interface has surface tension σ. Photos courtesy of Cohen & Nagel [4]. (b) Schematic of the numerical model. The suspended tube in the experiment is modeled by a point sink at height S. The closed surface used in the boundary integral simulation is the combination of I_f, the portion of the interface within the pinning radius a, and I_b, a back-surface mimicking the effect of a deep lower layer.

the interface is weakly deflected from being flat, instead of the small area near the tip of the hump where the interface is most distorted. This weakly deflected area is a region where the interface shape is insensitive to the lower-layer flow. In other words, when the axisymmetric hump solution fails, it does not fail at the tip, but instead comes apart everywhere at once. These observations allow us to propose a new scaling law for Q_c, one which successfully collapses all the data, both numerical and experiment, onto a single curve. From a practical view point, an understanding of the mechanism controlling Q_c is relevant for many applications, ranging from the encapsulation of biological cells for transplant therapy [12,13] to microfludic devices that use flow-focusing to create thin fibers, droplets, or compound drops [14–17].

Figure 1(b) illustrates the minimal model of viscous withdrawal we use to analyze the steady-state surface evolution. The axisymmetric withdrawal flow created by the suspended tube in the experiment is idealized as a point sink of strength Q located a height S above the undisturbed interface. We use a cylindrical coordinate system where r is the radial distance from the symmetry axis and z the height above the undisturbed interface. At a large radial distance $r = a$, the fluid interface I_f is "pinned," i.e., required to have zero deflection. We mimic the effect of a deep lower layer by requiring that a constant pressure jump, of size p_0, be maintained across the internal fluid surface I_b. A previous study [11] has tested this model extensively against the experimental situation and found that it reproduces the measured dynamics, with the model parameter p_0 and the pinning condition, having little effect on the outcome. Here, we focus on the results for Q_c.

We can estimate the strength of the two feedback mechanisms, the first coupling the interface deformation to the withdrawal flow, and the second coupling the lower-layer flow with the upper-layer flow, in terms of dimensionless parameters. At the interface, the imposed withdrawal flow has the approximate speed $Q/(4\pi S^2)$. Since viscous effects dominate over inertia in both layers in the experiment, the interface deformation occurs with speed σ/μ, where σ is surface tension and μ the viscosity of the liquid in the upper layer. Thus, the withdrawal flow is strong relative to the effect of the surface tension when the dimensionless capillary number $\mathrm{Ca} = \mu Q/(4\pi\sigma S^2)$ is large. The ratio of the lower-layer viscosity relative to the upper-layer viscosity, μ_0/μ, characterize the interaction between the induced recirculation in the lower-layer and the imposed withdrawal flow in the upper layer. We will see that Ca is a key control parameter while μ_0/μ is not. In addition, the fluid interface must also satisfy the constraint that it merges smoothly onto the flat, undisturbed profile in the far field. In our model, we can characterize this essentially geometric condition with the ratio S/a. When S is much smaller than a, the pinning is unimportant. In the withdrawal experiments, the interface is "pinned" at large distances by stratification so an analogous ratio is S_p/ℓ_σ, where $\ell_\sigma \equiv \sqrt{\sigma/\Delta\rho g}$ is the capillary length scale. Here, $\Delta\rho$ is the density difference between the two liquid layers and g is the acceleration due to gravity. The capillary length scale roughly corresponds to the radial distance beyond which the effects of hydrostatics dominate over surface tension.

We approximate the flows in both layers as purely viscous. The bulk flow in both layers then satisfies the linear Stokes flow equations, which we solve using a Green's function formulation [18]. The numerical formulation follows that devised by Kleine Berkenbusch, Cohen, & Zhang, and the full description can be found in the earlier study [11]. The key steps are that we first obtain an expression for the velocity on the fluid interface as an integral over a closed surface formed by the fluid interface, I_f and the back surface I_b. We then update the interface position via the kinematic condition requiring that a material point on the surface moves with the velocity on the surface. This procedure is repeated until either the normal velocity on the interface approaches 0, signaling convergence onto a steady-state hump solution, or until the interface becomes so deformed that it develops a finger that extends until it touches the point sink.

We characterize the overall shape evolution by plotting the hump height H against the withdrawal flux Q [Fig. 2(a)]. To simplify the discussion of the numerical results, we nondimensionalize the length-scales by the pinning radius a and the withdrawal flux by the character-

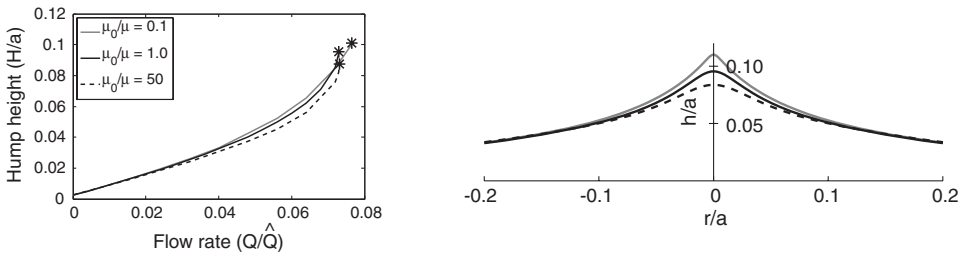

FIG. 2. Evolution of steady hump solutions. (a) Hump height H/a vs withdrawal flux $Q/\hat{Q}$. The asterisks indicate the end of selective withdrawal. (b) Close up of the steady hump shape at Q_c. The interface in the numerical model extends to the pinning radius $r/a = 1$.

istic scale $\hat{Q} \equiv \sigma a^2/\mu$. We show three $H(Q)$ curves, corresponding to $\mu_0/\mu = 0.1$, 1 and 50; the sink was held at the same height of $S/a = 0.2$ for all three runs. The end of the selective withdrawal regime in each set is marked by an asterisk. In all the cases presented, the hump height H increases as Q increases, eventually saturating as $\sqrt{Q_c - Q}$ at a finite value H_c when Q approaches Q_c. Similarly, the hump curvature κ saturates at a finite maximum curvature k_c (data not shown). These results are entirely consistent with results for equal-viscosity withdrawal [11]. Changing the relative viscosity ratio of the two layers, therefore, does not change the nature of the transition. The hump solution still disappears via a discontinuous saddle-node bifurcation. Consistent with previous results for emulsification of viscous liquid drops [19–21], the threshold withdrawal flux Q_c has a nonmonotonic variation with the viscosity ratio μ_0/μ. When the lower layer is made more viscous, increasing μ_0/μ from 1 to 50, the dimensionless threshold $Q_c/\hat{Q}$ increases from 0.0730 ± 10^{-4} to 0.0731 ± 10^{-4}. Decreasing the viscosity of the lower layer, so that $\mu_0/\mu = 0.1$, increases $Q_c/\hat{Q}$ to 0.0779 ± 10^{-4}. What is not expected is the very weak dependence of $Q_c/\hat{Q}$ on the viscosity ratio μ_0/μ, or equivalently, how close the different $H(Q)$ curves are to each other. These features suggest that changing the viscosity ratio μ_0/μ produces essentially the same sequence of steady-state shapes, and thus terminate at the same point.

The close-up profiles of the hump shapes at Q_c for the 3 runs with $\mu_0/\mu = 0.1$, 1, and 50 in Fig. 2(b) provide further support for this view. Except for a small region near the tip of the hump, the three shapes essentially coincide. In fact, the only quantity affected by μ_0/μ is the tip curvature. The dimensionless curvature of the hump tip at transition κ_c increases significantly as μ_0/μ decreases. Starting with a value of 38 ± 1 for $\mu_0/\mu = 50$, it increases to 70 ± 1 at $\mu_0/\mu = 1$, and then to $\kappa_c = 285 \pm 5$ at $\mu_0/\mu = 0.1$.

The fact that a dramatic change in κ_c produces essentially no change in Q_c suggests that the sharpening of the hump tip is not important in causing the selective withdrawal regime to end. This is rather surprising, as the withdrawal flow and the distortion are both strongest at the tip. One might then expect local weakening at the tip to be the most natural mode for the hump solution to fail. When a viscous flow begins to entrain a thin film of air, which correspond to a 2D analog of the axisymmetric process examined here, the interface does fail first at the tip [14].

To understand why axisymmetric withdrawal produces a different outcome, we estimate the contributions to the downwards force exerted by surface tension from different regions on the interface. Consider a hump with height H and curvature κ that extends over a radial distance L. Away from the tip, the interface is weakly deflected, with curvature scaling as H/L^2. Thus, this region contributes a force $F_L \approx \sigma(H/L^2)\pi L^2$. At the hump tip, however, the surface is approximately a half-sphere with radius $1/\kappa$. Surface tension pulls downwards with force $F_\kappa \approx (\sigma\kappa)2\pi(1/\kappa)^2$. Since F_κ scales as $1/\kappa$ while F_L scales as H, the downward force exerted by surface tension is dominated by the broader, weakly deflected region when $H\kappa > 1$. This is exactly what axisymmetric withdrawal produces. For all μ_0/μ, the steady interface always evolves until $H\kappa$ is larger than 1 so that the dominant contribution to the stabilizing force comes from the large region where the interface is only weakly deflected and thus insensitive to the lower-layer flow. A different failure mode is relevant in 2D air entrainment. In that case, F_L scales as $\sigma(H/L)$ while $F_\kappa \approx 2\sigma$, and the interface fails before H/L becomes much larger than 1, so that the tip region is always important. As a consequence, the lower layer flow is also important.

We next estimate Q_c using the idea that the hump solution fails when the upwards force exerted by the withdrawal flow in the upper layer overcomes the downwards pull of surface tension. The lower-layer flow is assumed to have no effect on Q_c. The viscous stress due to the withdrawal flow scales as $\mu Q/[4\pi(S-H)^2 H]$. Integrating over the area where the interface is weakly deflected, we find that $F_\mu \approx \mu Q L^2/[(S-H)^2 H]$. Finally, we know from the simulations that the smaller of the two imposed

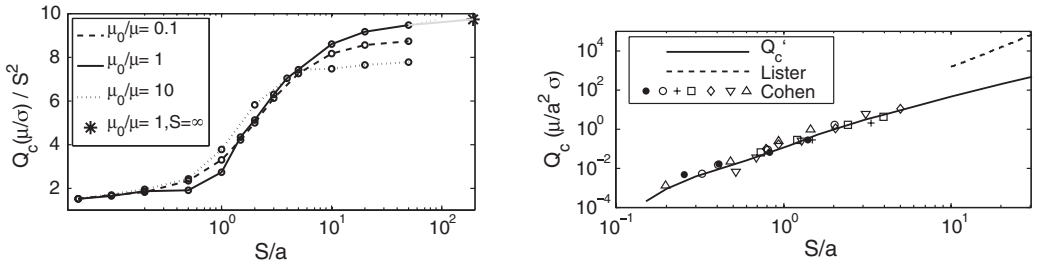

FIG. 3. (a) Rescaled threshold $Q_c(\mu/\sigma)/S^2$ as a function of S/a, for three values of μ_0/μ. The asterisk corresponds to the rescaled threshold withdrawal flux for an interface deformed by a uniform flow. (b) Rescaled measurements for $\mu_0/\mu = 0.001$ (solid circle), 0.0013 (cross), 0.006 (open circle), 0.021 (upper triangle), 0.3 (square), 1.26 (diamond), and 1.7 (lower triangle). All data from [4]. The dashed line indicates numerical results for $\mu_0/\mu = 1$, $S \gg a$ by Lister [3].

length scales, a and S, controls all the interface deflection ([11] and data not shown). In other words, if $S/a \ll 1$, then both the hump height H and the radial extent L are proportional to S. Thus, F_μ simplifies to $\mu Q/S$. Balancing F_μ against F_L, which dominates the force exerted by surface tension, we find

$$Q_c \sim \pi(\sigma/\mu)S^2 \qquad S/a \ll 1. \tag{1}$$

This essentially says that the selective withdrawal ends when the capillary number Ca is $O(1)$, regardless of the value of μ_0/μ. In the opposite limit ($S/a \gg 1$), the interface lengths, H, L, and $1/\kappa$ all scale with the pinning radius a. The resultant estimate is

$$Q_c \sim \pi(\sigma/\mu)S^2 \qquad S/a \gg 1 \tag{2}$$

which is exactly the same scaling form as the estimate for $S/a \ll 1$. The only difference is the numerical value of the prefactor. In Fig. 3(a), we check these predictions explicitly against our simulations by rescaling the calculated Q_c by $(\sigma/\mu)S^2$ and plotting the outcome. Regardless of the viscosity ratio, the rescaled curve approaches constant, but different, values as $S \ll a$ and $S \gg a$

Next, we show that rescaling the measured values of Q_c reported in [10] by $(\sigma/\mu)S^2$ collapses the data onto a single curve. We connect the point-sink model problem [Fig. 1(b)] with the experiment by setting $a = \ell_\sigma$. We also relate the sink height S to the tube height S_p via the formula $S = S_p + d$, where d is the tube diameter. This adjustment formula essentially assumes that the converging flow experienced by the interface is that produced by a point sink located at a distance of one tube diameter above the tube opening. Figure 3(b) shows the comparison after the rescaling. All the data from the experiment, which range in viscosity ratio from $\mu_0/\mu = 10^{-3}$ to $\mu_0/\mu = 1$, as well as all the data from the simulations ranging from $0.1 \leq \mu_0/\mu \leq 50$ collapse onto a single curve. Moreover, as S/a becomes small, the curve approaches a S^2 scaling form.

The puzzling trend reported by Cohen that half of the data set show a S^3 scaling is a consequence of the data being taken in the regime $S/a \approx 1$, so that $Q_c(S)$ is changing from one asymptotic trend to a different one. For completeness, we have also included numerical results by Lister [3]. He simulated equal-viscosity withdrawal in the context of geophysical flows, for which the capillary length scale ℓ_σ is much smaller than the sink height S. As a result, a very different constraint condition was used on the far-field interface. The comparison shows clearly that the regime analyzed by Lister is outside the regime of the withdrawal experiment by Cohen, which is why the S^3 scaling predicted by Lister does not appear in the final result.

In conclusion, we analyzed the nonequilibrium flow-driven transition from selective withdrawal to viscous entrainment using a combination of simulations, scaling estimate, and comparison with previous experiments. The flow in the lower layer has a largely passive role, affecting only how sharply curved the tip of the hump can become before the transition occurs. As a result, the steady-state surface evolves through basically the same sequence of shapes as Q increases. Transition is controlled by a global force balance, taking place when the upwards force exerted by the withdrawal flow overcomes the downwards force due to surface tension.

We thank Itai Cohen, Sarah Case, and Sidney R. Nagel for encouragement and advice. This research was supported by NSF Contract No. CBET-0730629 (W. W. Z.).

*Now at School of Natural Sciences, University of California Merced, Merced, CA, 95343 USA. fblanchette@ucmerced.edu

[1] D. Bensimon, L. P. Kadanoff, S. Liang, B. I. Schraiman, and C. Tang, Rev. Mod. Phys. **58**, 977 (1986).
[2] G. N. Ivey and S. Blake, J. Fluid Mech. **161**, 115 (1985).
[3] J. R. Lister, J. Fluid Mech. **198**, 231 (1989).
[4] I. Cohen and S. R. Nagel, Phys. Rev. Lett. **88**, 074501 (2002).
[5] W. W. Zhang, Phys. Rev. Lett. **93**, 184502 (2004).
[6] X. D. Shi, M. P. Brenner, and S. R. Nagel, Science **265**, 219 (1994).
[7] J. Eggers, Rev. Mod. Phys. **69**, 865 (1997).
[8] P. Doshi, I. Cohen, W. W. Zhang, M. Siegel, P. Howell, O. Basaran, and S. R. Nagel, Science **302**, 1185 (2003).
[9] N. C. Keim, P. Moller, W. W. Zhang, and S. R. Nagel, Phys. Rev. Lett. **97**, 144503 (2006).
[10] I. Cohen, Phys. Rev. E **70**, 026302 (2004).
[11] M. Kleine Berkenbusch, I. Cohen, and W. W. Zhang, J. Fluid Mech. **613**, 171 (2008).
[12] I. Cohen, H. Li, J. L. Hougland, M. Mrksich, and S. R. Nagel, Science **292**, 265 (2001).
[13] J. L. Wyman *et al.*, Small **3**, 683 (2007).
[14] A. M. Ganan-Calvo, Phys. Rev. Lett. **80**, 285 (1998).
[15] S. L. Anna, N. Bontoux, and H. A. Stone, Appl. Phys. Lett. **82**, 364 (2003).
[16] A. S. Utada, E. Lorenceau, D. R. Link, P. D. Kaplan, H. A. Stone, and D. A. Weitz, Science **308**, 537 (2005).
[17] A. G. Marin, I. G. Loscertales, M. Marquez, and A. Barrero, Phys. Rev. Lett. **98**, 014502 (2007).
[18] C. Pozrikidis, *Boundary Integral and Singularity Methods for Linearized Viscous Flow* (Cambridge University Press, Cambridge, 1992).
[19] G. I. Taylor, Proc. R. Soc. A **146**, 501 (1934).
[20] J. D. Buckmaster and J. E. Flaherty, J. Appl. Mech. **60**, 625 (1973).
[21] J. M. Rallison and A. Acrivos, J. Fluid Mech. **89**, 191 (1978).